# Quantification of Jet Flow by Momentum Analysis

## An In Vitro Color Doppler Flow Study

James D. Thomas, MD, Chun-Ming Liu, MD, Frank A. Flachskampf, MD, John P. O'Shea, MB, BS, Ravin Davidoff, MB, BCh, and Arthur E. Weyman, MD

**Previous investigations have shown that the size of a regurgitant jet as assessed by color Doppler flow mapping is independently affected by the flow rate and velocity (or driving pressure) of the jet. Fluid dynamics theory predicts that jet momentum (given by the orifice flow rate multiplied by velocity) should best predict the appearance of the jet in the receiving chamber and also that this momentum should remain constant throughout the jet. To test this hypothesis, we measured jet area versus driving pressure, flow rate, velocity, orifice area, and momentum and showed that momentum is the optimal jet parameter: jet area=1.25 (momentum)$^{.28}$, $r$=0.989, $p$<0.0001. However, the very curvilinear nature of this function indicated that chamber constraint strongly affected jet area, which limited the ability to predict jet momentum from observed jet area. To circumvent this limitation, we analyzed the velocities per se within the Doppler flow map. For jets formed by 1–81-mm Hg driving pressure through 0.005–0.5-cm$^2$ orifices, the velocity distribution confirmed the fluid dynamic prediction: Gaussian (bell-shaped) profiles across the jet at each level with the centerline velocity decaying inversely with distance from the orifice. Furthermore, momentum was calculated directly from the flow maps, which was relatively constant within the jet and in good agreement with the known jet momentum at the orifice ($r$=0.99). Finally, the measured momentum was divided by orifice velocity to yield an accurate estimate of the orifice flow rate ($r$=0.99). Momentum was also divided by the square of velocity to yield effective orifice area ($r$=0.84). We conclude that momentum is the single jet parameter that best predicts the color area displayed by Doppler flow mapping. Momentum can be measured directly from the velocities within the flow map, and when combined with orifice velocity, momentum provides an accurate estimate of flow rate and orifice area. (*Circulation* 1990;81:247–259)**



Color Doppler echocardiography flow mapping represents a major technologic breakthrough in displaying the spatial distribution of abnormal blood velocities that characterize valvular regurgitation.[1,2] However, the early hope for easy quantification of regurgitant flow with this technique has yet to be realized. One reason for this difficulty is that the appearance of the Doppler flow map depends on physical jet factors other than the regurgitant flow rate, per se. In particular, apparent jet size has been observed in vitro to increase with the driving pressure across the orifice, independent of the flow rate.[3–5] Thus, any theoretical framework for analysis of Doppler flow maps must characterize observed jets by a parameter that combines regurgitant flow rate and driving pressure.

A second major limitation of most current methods for quantifying regurgitation with Doppler color flow mapping is that they make only limited use of the data available within the flow map, typically using simple measurements of the width, length, and area of the regurgitant jet. By their nature, these Doppler analysis methods treat the color flow map as a binary quantity: flow is either present or absent, and no use is made of the actual velocities represented in the jet. Although these methods have been correlated with angiographic assessments of regurgitation,[6–9] neither approach provides a truly quantitative measure of

From the Noninvasive Cardiac Laboratory, Massachusetts General Hospital, Harvard Medical School, Boston, Massachusetts.

Presented in part at the 61st Annual Scientific Sessions of the American Heart Association, November 1988, Washington, DC.

Supported by grant 13-532-867 from the American Heart Association, Massachusetts Affiliate; J.D.T. was supported by the National Heart, Lung, and Blood Institute grant HL-07535; J.P.O. is a recipient of an Overseas Clinical Fellowship of the National Heart Foundation of Australia and the Athelston and Amy Saw Research Fellowship of the University of Western Australia.

Address for correspondence: James D. Thomas, MD, Noninvasive Cardiac Laboratory, Massachusetts General Hospital, Zero Emerson Place, Suite 2F, Boston, MA 02114.

Received January 9, 1989; revision accepted August 21, 1989.

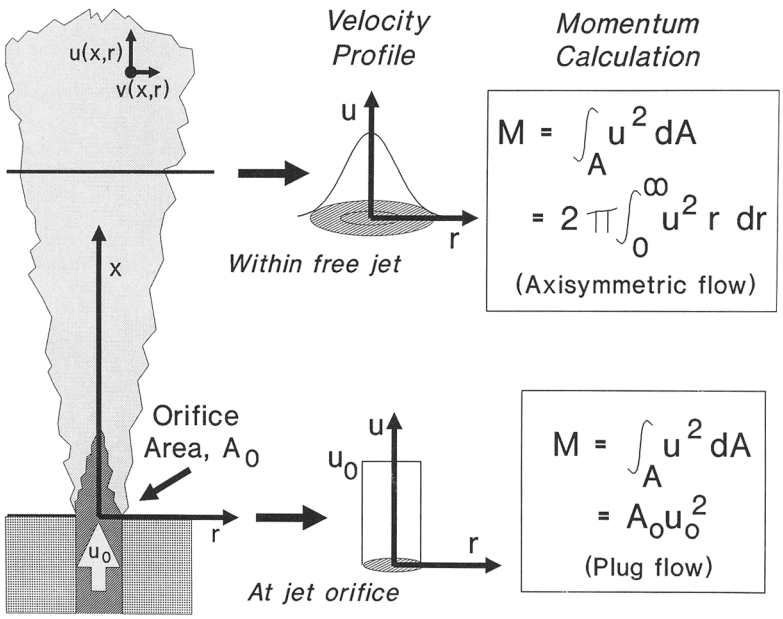


FIGURE 1. *Schematic diagram of axisymmetric, turbulent jet with momentum calculation. At left is the jet itself, with the* x *axis lying along the jet axis and the* r *coordinate specifying the radial distance from this central axis. The jet is formed by a plug of flow with velocity* $u_O$ *entering through a round orifice with area* $A_O$ *at bottom left; within the free jet, local velocity has an axial component* $u(x,r)$ *and radial component* $v(x,r)$*. In the center column are the velocity profiles transverse to the jet axis (u plotted against r) at the orifice level (bottom, plug flow) and within the free jet (top, Gaussian or bell-shaped curve). At right is shown the momentum calculation for these two levels. In general, the momentum flux crossing a given plane transverse to the jet axis is calculated by integrating* $u^2$ *across the particular plane:* $\int_A u^2\, dA$*. At the jet origin, the velocity profile is flat, and this integral is given simply by Equation 1B,* $A_o u_o^2$ *(equivalent to flow×velocity, Equation 1A). Within the free jet, the velocity profile is no longer flat; however, for a round orifice, it is axisymmetric, so velocity is a function of radial distance from the axis, and the momentum integral is* $2\pi \int_0^\infty u^2\, r\, dr$*.*

regurgitant flow. More sophisticated measurement would be possible if the velocity map were analyzed as a continuous quantity, with high-velocity regions given more weight than low-velocity regions. To be effective, however, any such analysis must use a theoretical framework based on fluid dynamics principles.

Fortunately, the general field of fluid dynamics and the specific topic of turbulent jet flow have received intense theoretical and experimental study during the past two centuries because of their importance in hydraulics, jet propulsion, and pollution control.[10,11] These studies have shown that the velocity distribution of the jet in the receiving chamber is best characterized by its momentum, a parameter that combines jet flow rate, driving pressure, orifice velocity, and orifice area into a single number.[12–15] In the absence of external pressure gradients, the momentum crossing a plane perpendicular to the jet axis should be the same at any point along the jet axis where it is measured.[16] Thus, if momentum can be quantified anywhere in the jet, it must be the same as the momentum entering the jet at its orifice. At the orifice, momentum is given by the product of jet velocity and the clinically relevant quantity of flow rate. Thus, by using jet momentum (measured anywhere within the Doppler flow map) and orifice velocity (measured by continuous wave Doppler), it may be possible to quantify the orifice flow rate.

The major hypotheses tested experimentally in this study were the following:

1) The jet parameter that best predicts the area displayed by color Doppler flow mapping is momentum, which combines flow rate, orifice area, driving pressure, and velocity into a single number and is fixed at the orifice.

2) Jet momentum may be calculated from the actual velocities within a color Doppler flow map and may be shown to be constant throughout the free portion of the jet.

3) If momentum can be quantified anywhere within the jet and if orifice velocity can be obtained by continuous wave Doppler, then the clinically relevant flow rate can be calculated as flow=momentum/velocity. The effective area of the jet orifice can be calculated as area=momentum/velocity.[2]

## Theoretical Background

The jet to be studied theoretically is formed by the constant discharge of blood with velocity $u_o$ through a circular orifice with an effective area of $A_o$ and flow rate $Q_o=A_o u_o$ (Figure 1; all mathematical symbols are defined in Table 1). If the Doppler transducer is assumed to align parallel to the jet axis, then the appearance of the jet will be determined by this axial velocity as a function of x and r: u(x,r). Radial velocity [v(x,r)] will be ignored because it is orthogonal to the Doppler beam.

### *Conservation Law Applied to Jets*

The jet may be thought of as a source for the transfer of mass, energy, and momentum into the receiving chamber, and conservation of these entities

**TABLE 1. Mathematical Symbols**

| | |
|---|---|
| $A_o$ | Effective jet orifice area ($cm^2$) |
| JA | Displayed color area of jet ($cm^2$) |
| L | Displayed length of free jet (cm) |
| M | Jet momentum flux ($cm^4/sec^2$) |
| $M_{SQ}$ | Square root of jet momentum (used in fitting Gaussian profiles to observed velocities, $cm^2/sec$) |
| p | Pressure (mm Hg or dynes/$cm^2$) |
| $\Delta p$ | Pressure gradient producing jet (mm Hg or dynes/$cm^2$) |
| $Q_o$ | Orifice flow rate ($cm^3/sec$) |
| r | Radial distance from the jet axis (cm) |
| $r_o$ | Effective jet orifice radius (cm) |
| $r_c$ | Local jet axis (used in fitting Gaussian profiles to jets, cm) |
| t | Time (sec) |
| u | Axial component of jet velocity (cm/sec) |
| $u_o$ | Jet velocity at the orifice (cm/sec) |
| $u_c$ | Low-velocity cutoff for display of color (cm/sec) |
| $u_m$ | Axial jet velocity along the central jet axis (cm/sec) |
| $u_N$ | Nyquist limit for velocity display (cm/sec) |
| v | Radial component of jet velocity (cm/sec) |
| x | Axial distance from jet orifice (cm) |
| $x_c$ | Length of receiving chamber, axial cutoff (cm) |
| $\alpha,\beta,\gamma$ | Coefficients for curve fitting |
| $\epsilon$ | Turbulent viscosity (relative to water=1) |
| $\rho$ | Blood density (1.05 $g/cm^3$) |
| $e$ | Base of natural logarithm, 2.71828 |



largely governs the behavior of the jet. Conservation of mass and energy are familiar from the continuity and Bernoulli equations, respectively, but momentum may be less so.

In rigid body mechanics (e.g., the flight of a baseball), momentum is defined as mass multiplied by velocity, and its change must precisely reflect applied forces (such as gravity) as specified by Newton's second law of motion:

force = mass × acceleration ≡ dM/dt (rate of change of momentum).

In fluid dynamics, we typically speak of momentum flux, the amount of momentum passing through a plane per unit time. (In this paper, "momentum" and "momentum flux" are used synonymously unless stated otherwise.) For the jet in Figure 1, the axial component of momentum is given by flow multiplied by axial velocity, or $Q_o u_o$.* Conservation of momentum dictates that the total momentum flux crossing any transverse plane orthogonal to the jet axis must be constant throughout the full extent of the jet.

*Calculation of momentum.* At the jet origin, momentum is expressible in many different ways, by combining the fundamental definition ($M=Q_o u_o$) with the continuity equation ($Q_o=A_o u_o$) and the Bernoulli equation ($\Delta p=\frac{1}{2}\rho u_o^2$, with pressure expressed in metric units, 1 mm Hg = 1,333 dynes/$cm^2$):

$$M=Q_o u_o \quad (1A)$$

$$=A_o u_o^2 \quad (1B)$$

$$=Q_o^2/A_o \quad (1C)$$

$$=2A_o\Delta p/\rho \quad (1D)$$

$$=Q_o\sqrt{2\Delta p/\rho} \quad (1E)$$

Equations 1A and 1B are especially interesting. They imply that if the momentum of the jet and its velocity at the origin are known (obtained, for instance, by continuous wave Doppler), one should be able to derive the jet flow rate (Equation 1A) and effective regurgitant orifice area (Equation 1B).

Note that Equations 1A–E are valid only for plug flow and so do not apply beyond the jet orifice where the velocity profile is not flat. Therefore, to calculate the momentum passing through an arbitrary plane orthogonal to the jet axis, we must generalize Equation 1B and integrate $u^2$ across the face of the jet:

$$M=\int_A u^2\,dA$$

For the special case of an axisymmetric jet, we may replace dA as shown with the circular rim $2\pi r\,dr$ and

*Alternatively, fluid density ($\rho$) may be included as $M=\rho Q_o u_o$. Because blood is incompressible (therefore, $\rho$ is constant), either definition is acceptable.

integrate from the center of the jet to the periphery as shown in Figure 1:

$$M=2\pi \int_0^* u^2 \, r \, dr \qquad (2)$$

*Jet velocity distribution.* In the absence of an external pressure gradient, momentum flux throughout the jet retains its orifice value. Applying this conservation principle to simplified versions of the Navier-Stokes equations permits an approximate description of the velocity distribution for a turbulent jet[15]:

$$u(x,r)=\frac{7.8\sqrt{M}}{x} e^{-94(r/x)^2}* \qquad (3)$$

Thus, the velocity along the center axis where r is equal to 0 ($u_m$) decreases inversely with distance from the jet origin ($u_m=7.8\sqrt{M}/x$), and the velocity profile across the jet is a Gaussian (bell-shaped) curve:

$$u(r)=u_m e^{-94(r/x)^2} \qquad (4)$$

where $u_m$ is the centerline velocity at a given distance, x, from the orifice.

Equation 3 holds for turbulent rather than laminar jets, a transition governed by the jet Reynolds number, $Re=u_o d_o/\nu$, where $d_o$ is the orifice diameter, and $\nu$ is the kinematic viscosity. In constrained pipe flow, turbulence begins at about Re=2,300. For free jets formed by abrupt stenoses, turbulence occurs much sooner, with instabilities noted as low as Re=250[17] and turbulence at Re=450.[18] A recent study shows abrupt onset of turbulence at Re=500.[19]

Importantly, Equation 3 contains no reference to fluid viscosity or the orifice velocity and flow rate. Far from the jet origin, there is no influence of the specific orifice shape, only the impact of turbulent properties and total jet momentum.[20]

## Methods

The three theoretical predictions were tested using Doppler color flow mapping of in vitro models of valvular regurgitation.

### *Data Acquisition and Initial Processing*

*In vitro model 1.* For this study, we primarily used a previously described 57 cm (H)×8 cm(W)×14 cm (L) Plexiglas model of the heart to simulate regurgitant flow.[21,22] This model is divided into two chambers by a vertical septum, at the bottom of which is a mount for valvular orifices. After a pressure gradient was established between the two chambers, blood was allowed to flow by gravity into the receiving chamber.

A very useful aspect of this model is that within a single experimental run, it is possible to simulate a wide range of flow rates, driving pressure, and velocity. We have previously shown[21,22] that the pressure decay follows a predictable parabolic curve, whereas the flow and velocity decay curves are linear. Thus, by simply knowing the initial pressure gradient and the time elapsed to measurement, we can accurately predict the instantaneous flow rate, pressure, and momentum flux at any time during the decay.

For this study, we used circular orifices with areas of 0.1, 0.2, 0.3, and 0.5 $cm^2$. Data analysis for all experimental runs was performed from an initial pressure gradient of 10 mm Hg. This combination allowed the investigation of jets with the following features: pressure gradient, 0–10 mm Hg; orifice velocity, 0–158 cm/sec; orifice flow rate 0–60 $cm^3$/sec; and momentum, 0–9,400 $cm^4/sec^2$. Heparinized canine blood with a measured viscosity of 1.8 cP was used, yielding peak jet Reynolds numbers of 3,134, 4,433, 5,425, and 7,004 for the four orifices, respectively. We have reported that flows above Re=300 in this model have low-frequency velocity fluctuations about 20% of the mean velocity with full turbulence noted above Re=600,[23] supporting our use of Equation 3 in analyzing these data.

*In vitro model 2:* To examine jets with higher orifice velocities, we used a gravity-fed, constant flow model with pressure gradients as high as 81 mm Hg. Data were obtained for flow through 0.005-$cm^2$ and 0.1-$cm^2$ orifices at pressures between 18 and 81 mm Hg. Maximal jet velocity was 4.6 m/sec with momentum 18,900 $cm^4/sec^2$. Water (with cornstarch added for Doppler reflectivity) was used, yielding a peak Reynolds number of 14,416.

*Echocardiographic examination.* Doppler flow images were obtained with a Hewlett-Packard 77090 echocardiograph and recorded onto ½ in. videotape for subsequent analysis. Acquisition parameters included carrier frequencies of 3.5 and 5 MHz; depths between 6 and 20 cm, yielding Nyquist limits from 37 to 106 cm/sec; pure velocity display mode; large packet size; and gain optimized and left constant for the study. To examine the velocity decay along the jet centerline, pulsed Doppler recordings were obtained along the jet axis (guided by flow mapping) at distances of 1.5, 2.5, 3.5, 4.5, 5.5, and 6.5 cm from the orifice. Continuous wave Doppler was used to obtain the peak velocity across the orifice.

*Color Doppler processing.* The Doppler flow data from each recorded experimental run in model 1 was analyzed from the time of maximal momentum, flow, and pressure until equilibration between the two chambers occurred. Steady-state conditions were analyzed for data from model 2.

Jet area was measured in model 1 using an offline color analyzer (Sony). At 12–20 time points evenly spaced within the jet decay for each orifice, the visible jet was hand traced and the area was measured and recorded. The time interval from the start of each experimental run was also recorded to allow calculation of the instantaneous pressure gradient, orifice flow, and jet momentum corresponding to that jet area.

*This formula differs from others that have been published[15] in that we have substituted M from Equation 1B and have used the area of the vena contracta instead of the anatomic area.

The actual velocities within the jet were quantified using a D-200 Off-line Analysis System (Dextra Medical, Long Beach, California). For each experimental run in model 1, six to eight video frames were digitized, and a rectangular region of interest was marked off that enclosed the jet. In model 2, representative frames were analyzed for each level of driving pressure. The color values for each pixel within the region of interest were then compared with a look-up table derived from the color calibration bar on the videotape,[24] and the calculated velocities were written to a computer disk in ASCII format. Subsequent analysis of the velocity data was performed using customized software written with the ASYST Scientific Analysis Package (Macmillan Software Publishing, New York).

*Hypothesis 1. Analysis of Jet Area Versus Flow Rate, Orifice Area, Pressure, and Momentum*

Data from experimental runs with the four orifice sizes in model 1 were pooled, producing a data set with measured jet area as the dependent variable and known flow rate, orifice velocity, driving pressure, orifice area, and momentum as independent (predictor) variables.

*Univariate analysis of jet area versus flow rate, pressure, and momentum.* Previous work in this laboratory[4,25] showed a nonlinear relation between observed jet area and orifice flow. It is also axiomatic that with no flow, no color should be seen. Accordingly a power law function passing through the origin was chosen as the mathematical modeling function: $y=\alpha x^{\beta}$, where y is observed jet area, x is the independent variable (flow, pressure, and momentum, in turn), and $\alpha$ and $\beta$ are fitting parameters to be determined. This fitting operation was performed using Marquardt nonlinear least-squares approximation[26] with the RS-1 data analysis program (Bolt, Beranek, and Newman, Cambridge, Massachusetts). The optimal jet parameter (of flow rate, pressure, and momentum) was chosen as the one that yielded the highest correlation with the observed jet area.

*Analysis of covariance.* Again based on prior observation,[4,5] we postulated that distinct functional relations between jet area and flow would be observed for each orifice area. Similarly the relation between jet area and driving pressure was expected to depend on the orifice area. However, if momentum were indeed the optimal jet parameter to predict its appearance, then orifice area should not effect the relation. Accordingly, analysis of covariance was performed with jet area as the dependent variable; orifice area as the grouping variable; and flow rate, pressure gradient, and momentum, in turn, as the covariate (BMDP program P1V). The dependent variable and each of the covariates were log-transformed to better model the power-law function used above. Orifice area was considered to have a significant impact on a given jet area–covariate relation if the adjusted group means differed with a significance of $p<0.05$.

*Optimizing the combination of flow rate, velocity, pressure, and orifice area to predict jet area.* The final analysis of the jet area data was to determine whether the combinations of flow rate, velocity, pressure gradient, and orifice area that best predicted jet area were the same as those in Equation 1 used to define jet momentum. For instance, the mathematical model of jet area (JA) as a function of velocity and orifice area was $JA=\alpha A_o^{\beta} u_o^{\gamma}$. Obtaining the logarithm of both sides produced an expression solvable by multilinear regression: $\ln(JA)=\ln(\alpha)+\beta\ln(A_o)+\gamma\ln(u_o)$. If the ratio between the exponents $\beta$ and $\gamma$ were not significantly different from the ratio used to define momentum in Equation 1 (in this case, $\gamma/\beta$ should be 2 according to Equation 1B), then the momentum combination was taken to be the optimal one. This test was conducted for each of the five combinations used in Equations 1A–E.

*Hypotheses 2 and 3. Analysis of Actual Velocities Within Flow Maps*

*General velocity analysis.* Each velocity map output from the jet region of interest was a rectangular array of numbers corresponding to the axial velocities, $u_{i,j}$, with the rows (i index) arranged perpendicular to the jet axis and the columns (j index) arranged parallel to the axis. By knowing the pixel calibration from the video screen (horizontally and vertically) and the position of the region of interest relative to the jet orifice, we could consider $u_{i,j}$ as discrete samples from the velocity distribution of the jet, u(x,r). These ASCII files were read by the ASYST customized software for further analysis.

Because of the low Nyquist velocities ($u_N$) present in the Doppler flow maps, many of the jets had aliased velocities within them. Because bulk flow was always toward the transducer, any negative velocities observed within the jet were assumed to be aliased and were corrected by adding their observed negative values to $2u_N$. No attempt was made to analyze velocities very close to the orifice where multiple aliasing occurred. Finally, low-speed negative velocities seen outside the jet were believed to be true counterflow and were not included in the jet analysis.

*Overall jet structure.* The accuracy of Equation 3 in describing jet velocity distribution was tested in two ways. First, the centerline velocity ($u_m$) was measured by pulsed Doppler at 1-cm intervals and compared with the orifice velocity ($u_0$, obtained by continuous wave Doppler) for 20 levels of jet momentum. These data were fit to an inverse function predicted by Equation 3: $u_m/u_o=\alpha/(x+\beta)$. The offset parameter, $\beta$, was included because turbulent jets typically behave as if they originate from a pointlike "virtual orifice" slightly inside the proximal chamber.[15] Second, we tested velocity profiles transverse to the jet axis for their expected Gaussian shape. Data from single rows of the color velocity map (corresponding to a plane transverse to the jet axis at a distance $x_o$ from the orifice) were fit to a formula suggested by Equation 3: $u(x_o,r)=7.8M_{SQ}/\epsilon x_o\ e^{-94[(r-r_c)/\epsilon x_o]^2}$, where the

parameters to be fit are $M_{SQ}$, the square root of the jet momentum; $r_c$, the location of the jet axis within the velocity map (to allow for slight random deviations of the local jet axis from the overall axis; and $\epsilon$, a term related to the "turbulent viscosity" of blood, expressed as a ratio relative to that of water. Turbulent jet theory predicts that this term should be independent of the actual fluid, and thus, it was expected that $\epsilon$ would be approximately 1. For each digitized jet, a number of profiles from different values of x were fit by this procedure. The fitted $M_{SQ}$ was compared with the square root of the known momentum, and $\epsilon$ was compared with the expected value of 1.

*Hypothesis 2. Calculating momentum directly from observed velocity.* Momentum was calculated directly from the observed velocity with Equation 2, with two minor modifications. First, the local jet axis swings left to right randomly, so the local jet centroid (as a function of axial distance from the orifice) was calculated to establish the center around which to assume axial symmetry in calculating momentum:

$$r_c(x)=\int_{-\infty}^{\infty} r\,u(x,r)\,dr \Big/ \int_{-\infty}^{\infty} u(x,r)\,dr.$$

The second modification to Equation 2 was to integrate the profile on both sides of the jet axis to use all of the available data: $M(x) = \pi \int_{-\infty}^{\infty} u^2(x,r)\,[r-r_c(x)]\,dr$. M(x) was calculated for each row in the jet region of interest. From a 2–3-cm segment along the jet axis (40–100 rows of data, depending on depth), mean momentum ($\overline{M}$) was calculated for comparison (by linear regression) with true momentum, and standard deviation was calculated as a measure of jet turbulence.

*Hypothesis 3. Use of momentum to calculate orifice flow rate and effective orifice area.* Orifice velocity ($u_o$) corresponding to the momentum calculations above was measured with continuous wave Doppler in model 2. For model 1, orifice velocity was recorded during repeated experimental runs identical to those used for color Doppler acquisition. These velocity data were then combined with the corresponding mean jet momenta to yield orifice flow rate ($Q_o$) as suggested by Equation 1A: $Q_o=\overline{M}/u_o$. The estimated orifice flow rates from all of the jets analyzed were then compared with the known flow rates by linear regression. Similarly, effective orifice area ($A_o$) was calculated using Equation 1B: $A_o=\overline{M}/u_o^2$. These effective areas were compared with the physical orifice area by linear regression.

*Analytical Summary*

The jets generated for this study were analyzed both as binary and continuous flow maps. For binary analysis, jet size was measured, and the best univariate predictor was selected from among flow rate, driving pressure, and momentum. Bivariate models with various combinations of flow, pressure, velocity, and orifice area were also tested to determine whether any could improve on the predictions provided by momentum alone.

To analyze the jet velocity as a continuous variable, the observed jet velocity was assessed for compatibility with the predicted inverse decay along the jet axis and Gaussian profile across the axis. The transverse profiles were also used to calculate momentum directly, which was compared with the known momentum of the jet. Finally, these momenta were divided by jet velocity to yield estimates of orifice flow rate, which was compared with the known flow rate and were divided by velocity squared to give an estimate for the effective orifice area.

## Results

*Hypothesis 1. Analysis of Jet Area*

Figure 2 shows measured jet areas plotted as functions of flow rate (Figure 2A), pressure gradient (Figure 2B), and momentum (Figure 2C). The same data are plotted in each graph; only the parameter chosen for the *x* axis is different. In each case, the data are stratified by the orifice area that produced the jet. Figure 2A shows that for a given flow rate, jets issuing from small orifice areas were considerably larger than those from the larger orifices (because the small orifice jets had higher velocity). Similarly, Figure 2B shows that for the same driving pressure, jets from larger orifices were larger (because the associated flow rate was larger).

*Optimal prediction for jet area using single variables.* Power-law fits derived with flow rate and driving pressure both show good correlation with the overall observed jet areas. With flow rate: $JA=3.12\ Q^{.40}$, $r=0.947$, SD regression=1.17. With driving pressure: $JA=6.92\ P^{.30}$, $r=0.900$, SD regression=1.59. With momentum as the independent variable, however, a better fit was obtained: $JA=1.25\ M^{.28}$, $r=0.989$, SD regression=0.53, indicating that momentum is superior to either flow or pressure in predicting jet appearance.

*Analysis of covariance.* Analysis of covariance on these data showed a very significant effect of orifice area ($p<0.0001$) on jet size when the covariate was flow rate (Figure 2A) or pressure (Figure 2B). However, when jet area was adjusted by jet momentum, the data from the four orifice sizes were superimposable (Figure 2C), and analysis of covariance showed no effect of orifice size independent of momentum ($p$=NS).

*Optimal bivariate prediction of jet area.* The jet area and all of the independent variables were log-transformed to convert the power-law fits into a multilinear regression problem. Again, momentum alone predicted the appearance of the jet as well as any combination of the other variables. Furthermore, when momentum was excluded from the analysis, the optimal combinations of the other variables were not found to be statistically different from Equations 1A–E and thus were not different from analysis with momentum alone. This is further evidence that

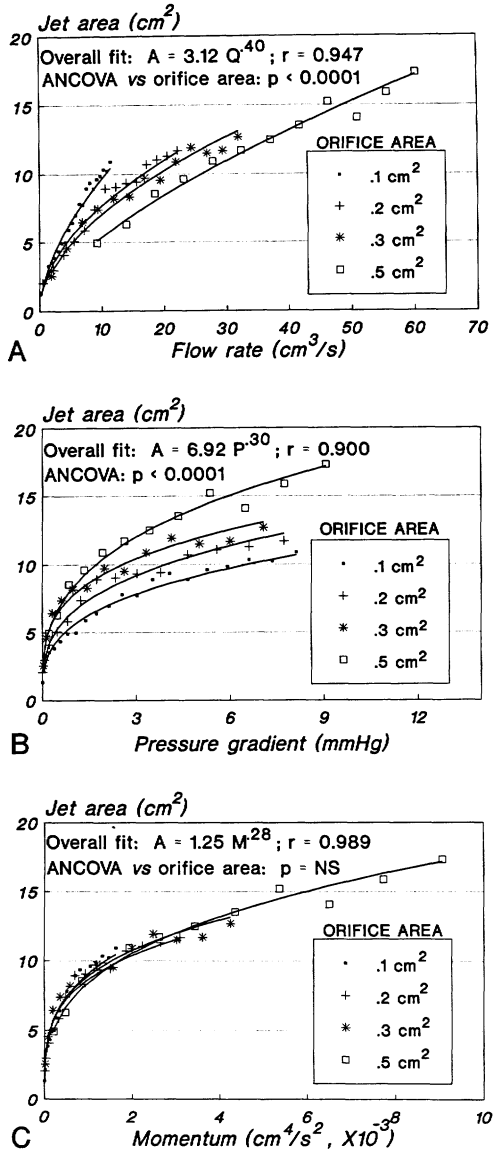


FIGURE 2. *Plots of measured jet area displayed as a function of jet flow rate* (Panel A), *driving pressure* (Panel B), *and momentum* (Panel C). *Each is stratified by the orifice area producing the jet. These show that both flow rate and pressure affect the jet appearance independently, but combining them into momentum, optimally characterizes the jet. A, measured jet area; Q, jet flow rate; P, orifice driving pressure; M, jet momentum; ANCOVA, analysis of covariance with orifice area as the grouping variable and flow rate (Panel A), pressure gradient (Panel B), and momentum (Panel C) as the covariate.*

momentum is indeed the jet parameter that best predicts the area displayed by Doppler flow mapping.

*Hypotheses 2 and 3. Analysis of Jet Velocities*

*General appearance of the jets.* Figure 3A shows the decay in centerline velocity along the jet axis pooled from 20 levels of jet momentum through the 0.1-cm² orifice. As predicted by Equation 3, $u_m$ decays inversely with x except for a plateau near the orifice where the jet core has not yet been obliterated.

Figures 3B, 3C, and 3D display transverse velocity profiles from the color flow maps of three jets. Also shown are the best-fitting Gaussian curves of the form predicted by Equation 4. Where the velocity was completely nonaliased (as in Figures 3B and 3C), the Gaussian fit in general was good, within the limitations of turbulent flow and the coarse velocity resolution of contemporary echocardiographs.

However, when velocity aliasing occurred (as in Figure 3D), attempts at unwrapping the velocity usually resulted in a marked discontinuity at the aliasing boundary. Though this artifact is certainly multifactorial in origin, one contributing cause appeared to be "leakage" between the red and blue video signals such that an individual pixel could have forward and reverse velocity data written in it. Despite this discontinuity, the Gaussian fits to unwrapped, aliased flow was reasonably good. Throughout a wide range of jet momenta, this Gaussian form fit the observed velocity profiles with an average correlation of $r=0.85$. Of note, the average turbulent viscosity, $\epsilon$, was 1.46, indicating that the jets spread about 46% faster than would have been expected for a free water jet. This may be due to some intrinsic difference between water and blood or due to the backflow of blood hitting the end of the chamber and increasing the shear rate of the periphery of the jet.

*Hypothesis 2. Direct calculation of momentum.* The digitized regions of interest were used to calculate momentum directly using Equation 2. To establish the proper local axis location around which to base the axisymmetric momentum calculation, a velocity centroid was calculated for each cross-sectional profile (with each jet having, typically, 80–150 profiles). On average, this centroid swung randomly 0.9 mm about the average axis as a function of axial distance, which was about 5–10% of the total jet width. This local centroid was then used to calculate the momentum. Figure 4 shows the typical appearance of jet momentum as a function of axial distance from the orifice along with the fluctuation in jet axis. For this jet, the mean axis lay along $r=0$. Although large scale fluctuations in measured jet momentum are evident, on average the momentum remained relatively constant, independent of distance from the orifice. Only within about 2 cm of the chamber wall did the momentum consistently decay, reaching 0 just at the chamber wall. Figure 5 compares measured mean momentum with the true momentum for 50 jets (33 from model 1, 17 from model 2), displaying good agreement. These data are pooled from both in vitro models because analysis of covariance disclosed no difference in relations between true and observed momentum. The major difficulty arose where multiple aliasing occurred in the core of some high-velocity jets, making accurate unwrapping impossible.

*Hypothesis 3. Calculating flow rate and effective orifice area from observed momentum.* Figure 6 displays the results of dividing the measured jet momenta by orifice velocity to derive the orifice flow rate (an inversion of Equation 1A). Jet velocity was measured

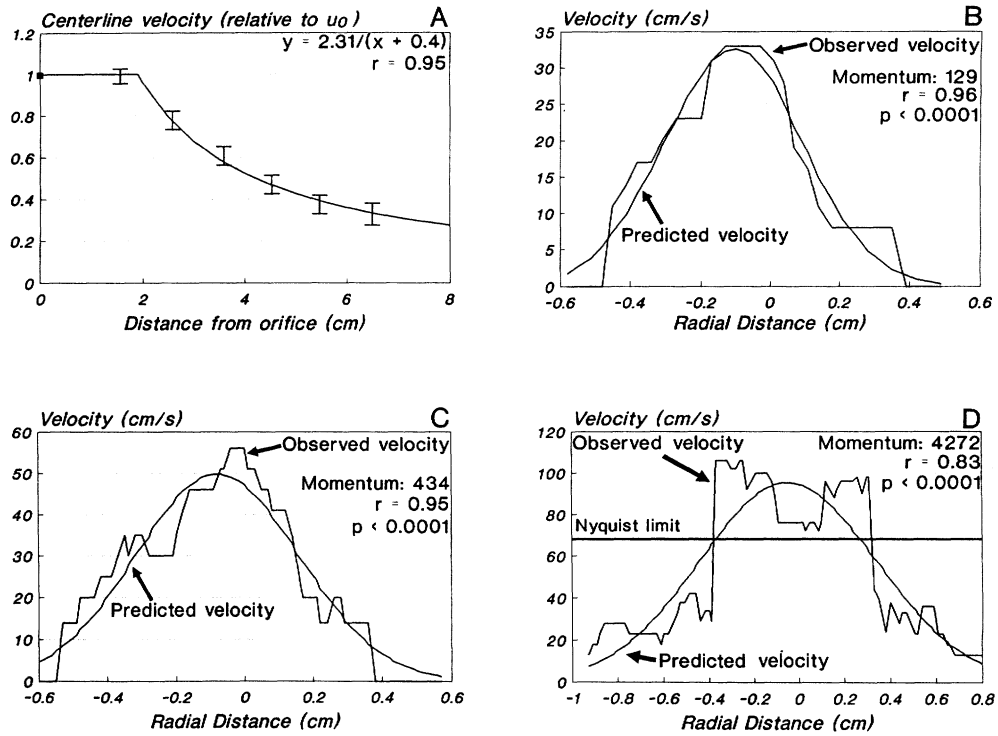


FIGURE 3. *Plots of observed spatial distribution of axial velocity within jets from the 0.1-cm² orifice.* Panel A: *Decay of centerline velocity as a function of axial distance. Data are pooled from 20 levels of driving pressure and are normalized to the respective orifice velocity.* Panels B, C, *and* D: *Jet cross-sectional profiles with theoretical Gaussian fits. For low-momentum jets (Panels B and C), the overall fit to the form of Equation 4 is good given the known jet turbulence and the coarse Doppler velocity measurements. In Panel D, velocities above 68 cm/sec were aliased, and attempts at "unwrapping" them resulted in a marked discontinuity at the aliasing boundary, reflecting leakage between the red and blue signals, in part due to limited color bandwidth of NTSC video.*



by continuous wave Doppler and by application of the Bernoulli relation to the pressure gradient measured in the flow models under conditions corresponding to the color jet analyzed. Again, good agreement is observed with the known orifice flow rate for both in vitro models.

A strong linear relation was observed between the true orifice area (x in the following regression equation)

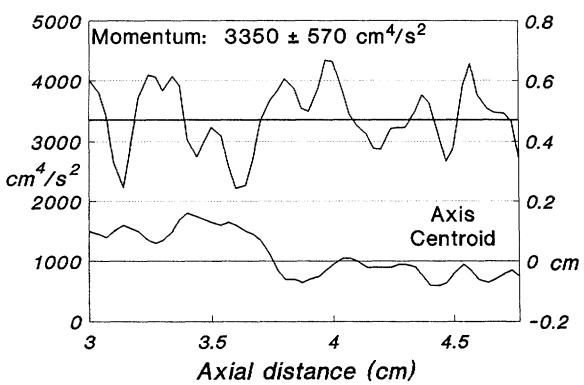


FIGURE 4. *Plot of jet momentum flux (left axis) and local axis location (right axis), each plotted against axial distance from the orifice for a single Doppler flow map frame. Random fluctuations in both are evident, but on average, momentum remained constant throughout the jet.*

and the effective orifice area calculated from the observed jet momenta and velocities: $y=0.82x+0.01$, $n=50$, $r=0.84$, $p<0.0001$. The slope of the line (0.82) corresponds approximately to the coefficient of discharge for the orifice.

## Discussion

We have shown that momentum flux, which combines orifice flow rate, velocity, driving pressure, and orifice area into a single number, is the best jet parameter for predicting its appearance by color Doppler flow mapping. We have also shown in vitro that it is feasible to measure momentum directly from Doppler flow maps and combine this with orifice velocity (measured by continuous wave Doppler) to estimate the orifice flow rate and the effective orifice area. These facts may have implications for the quantification of valvular regurgitation by Doppler mapping.

### *Analysis of Jet Area*

Most of the early clinical studies of color Doppler flow mapping correlated the length, width, or area of the color jet with semiquantitative measures of regurgitant severity such as angiography.[6-9] Although some clinically useful algorithms have been produced by this approach, subsequent in vitro work has shown that jet area is independently affected by jet flow rate and orifice velocity.[3-5] We have shown, however, that characterizing jets by their momentum (the product

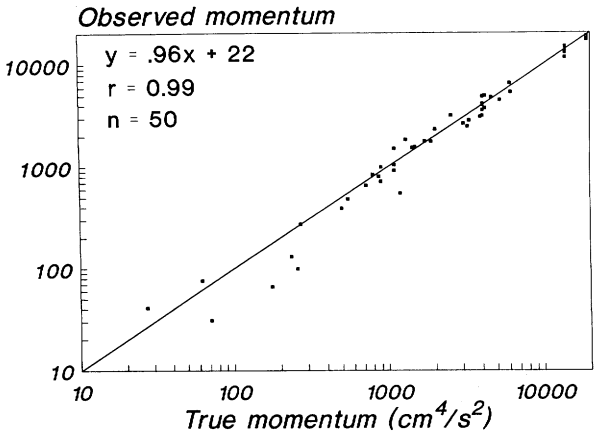


FIGURE 5. *Regression plot of mean jet momentum calculated from Doppler flow maps compared with true momentum. Equation 2 was applied to the jet region of interest and averaged along the jet axis. The line of identity is shown.*

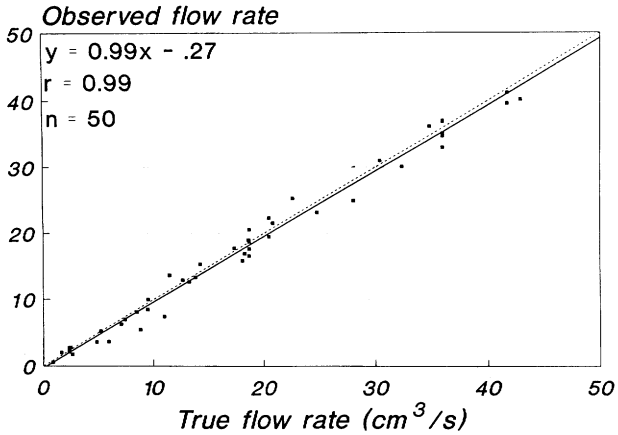


FIGURE 6. *Regression plot of jet flow rate calculated from Doppler flow maps compared with known orifice flow rate. Jet momentum was calculated by Equation 2, then divided by orifice velocity to yield flow rate (Equation 1A). Regression line, solid line; line of identity, dashed line.*

of flow rate and velocity) produced the optimal correlation with the observed jet area. Indeed, when jet area was plotted against momentum, data from a fivefold range of orifice sizes were superimposable. As shown in this study, the relation between momentum and jet area is a highly nonlinear power law function: $JA=1.25M^{.28}$.

Thus, momentum is the best jet parameter to predict jet area by color flow mapping. Unfortunately, other factors such as chamber constraint and machine gain significantly influence the jet appearance and may have more impact on jet area than on the actual momentum of the jet. This may be approached theoretically by considering the expected color area for jets of given momentum (M) entering a receiving chamber of length $x_c$ (the "cutoff" in the axial direction). The third parameter entering into this analysis (detailed in Appendix 1) is the lowest velocity for which the Doppler machine will show color, which is termed the low-velocity cutoff ($u_c$). If we assume the velocity within the receiving chamber is given by Equation 3, then color should be displayed wherever the velocity is greater than $u_c$. In fact, the current generation of color flow mappers do not have a sharp low-velocity cutoff analogous to the wall filter of pulsed Doppler. However, the gain setting will change the sensitivity of the instrument to low-velocity signals and thus has much the same effect.[27] Marked variation in displayed area (due presumably to changes in $u_c$) have been observed in vitro not only with variations in gain but also in carrier frequency, pulse repetition frequency, and frame rate.[27–29]

As shown in Appendix 1, the displayed length (and approximately the width) of an unconstrained jet varies directly with the square root of the jet momentum and inversely with $u_c$. Its area varies linearly with M and with the inverse square of $u_c$ (Equation A2). Thus, doubling the low-velocity cutoff decreases the displayed area by a factor of four. However, this dramatic dependence on $u_c$ is seen only for completely free jets. When the length of the receiving chamber is less than the potential length of the free jet, then the jet is constrained, and we must use Equation A3 to calculate its area. Figure 7A shows the effect of chamber constraint on displayed jet area. Here, the jet is constrained at 11 cm, similar to in vitro model 1, and the overall relation between momentum and displayed area is distinctly nonlinear. In fact, the shape of this curve is quite similar to that

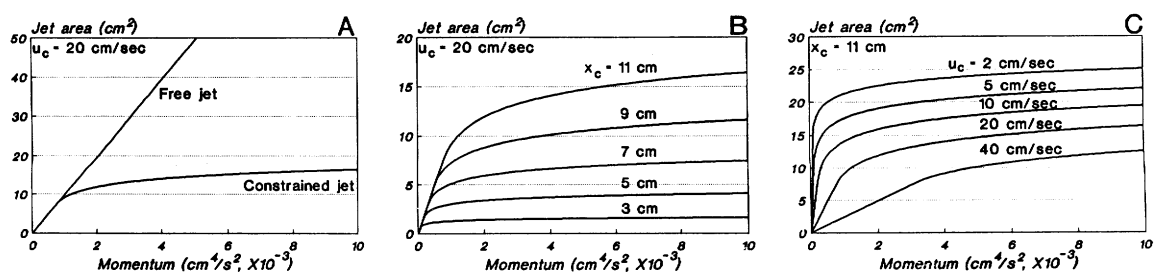


FIGURE 7. *Plots of effect of jet momentum, chamber constraint ($x_c$), and low-velocity cutoff ($u_c$) on displayed jet area.* Panel A: *For an unconstrained jet ($x_c=\infty$), area increases linearly with momentum. However, if the jet is truncated at $x_c=11$ cm, jet area rises very nonlinearly and is similar to the curve in Figure 2C.* Panel B: *Effect of receiving chamber length on displayed area. The top curve is the same as the constrained curve in Panel A.* Panel C: *Effect of low-velocity cutoff on displayed jet area for an 11-cm receiving chamber. The $u_c=20$ cm/sec curve is the same as in Panel A.*

in Figure 2C. Figure 7B shows the effect of changes in receiving chamber length ($x_c$=3, 5, 7, 9, and 11 cm) on the displayed area, whereas Figure 7C shows the influence of machine gain ($u_c$=2, 5, 10, 20, and 40 cm/sec) on the area of a jet constrained at 11 cm.

*Implications for using jet area to grade regurgitant severity.* The lesson from this is twofold: 1) jet momentum is the best independent jet variable to use in predicting color flow area; 2) however, the precise functional relation between momentum and jet area is unpredictable and depends heavily on the size of the receiving chamber and machine-dependent factors such as gain. Thus, no special import should be placed on the particular functional form found in our in vitro model, $JA=1.25\ M^{.28}$ because changes in $x_c$ and $u_c$ may be expected to affect both the exponent and multiplicative constant in this expression, and these precise interactions would have to be determined empirically for a given geometry-machine combination. Thus, it is unlikely that any relation will be found to relate simple jet area to true jet momentum (and by Equations 1A and 1B to jet flow rate and orifice area). This fundamental uncertainty in using simple jet area is what makes analyzing the velocities themselves within the jet such an attractive approach.

### *Analysis of Actual Velocities Within the Color Flow Map*

Analysis of simple jet area treats the color flow map as binary data: flow is either present (color shown) or not (no color shown). All of the actual velocity data within the color map are discarded in this analysis, data that we have examined by comparing the displayed color to the machine-generated color bar. Although this approach is indirect (far better to analyze the digital velocity data before color encoding), we confirmed that the color-derived velocities within turbulent jets were consistent with the predictions of Equation 3: the centerline velocity decays inversely with axial distance, and the velocity profile across the jet axis is Gaussian in shape.

*Advantages of momentum analysis in Doppler jet analysis.* Our overall strategy for analyzing these jets was based on quantifying momentum flux within the jet. Momentum flux is especially attractive for analyzing Doppler flow maps of jets for several reasons. First, momentum exists only in one form, not like energy that is convertible from kinetic energy (measurable by Doppler) to heat (unmeasurable by Doppler). Second, momentum is a vector quantity. That is, it has components along each of the three coordinate directions, and each of these component momenta must be conserved. This is important because Doppler measures only the component of velocity parallel to the ultrasound beam and because the momentum measured with this component must remain constant throughout the jet. Finally, we can combine momentum with orifice velocity (readily measured by continuous wave Doppler) to estimate regurgitant flow rate ($Q_o=M/u_o$) and effective orifice area ($A_o=M/u_o^2$).

*Application of the method to quantification of valvular regurgitation.* The findings of this study have implications for the use of Doppler flow mapping in the assessment of valvular regurgitation. If it were possible to quantify momentum within a clinical jet and divide this by the orifice velocity from the same time in the cardiac cycle, this should yield the instantaneous regurgitant flow rate. Repeating this process throughout the time of regurgitation would then yield flow as a function of time [Q(t)], which could be integrated to give regurgitant stroke volume: $\int Q(t)\ dt$. This approach could be simplified if it were possible to assume the regurgitant orifice area to be constant throughout the regurgitant time period. Then, the effective area could be found at a single point in the cardiac cycle (usually at the time of the largest jet) and multiplied by the orifice time velocity integral to give regurgitant stroke volume: $(M/u_o^2)\ \int u_o(t)\ dt$. Furthermore, the effective regurgitant orifice area itself would be of clinical relevance because it may represent a load-independent measure of the fundamental valve disease process.

*Study limitations.* It must be emphasized that these techniques have been validated for a very artificial in vitro situation; clinical applicability has not yet been shown. Furthermore, even in this idealized setting, several potential limitations were encountered because of the turbulent nature of the jets and the limitations of current color Doppler flow mapping technology. The velocity variance within turbulent jets has been observed to average from 20% to 25% of the local mean velocity.[11,23] Thus, one may expect a similar degree of variation in measured momentum crossing individual planes within the jet. Beyond this true variance, we observed further variation in measured momentum due to the random instantaneous swings in the local jet axis that significantly altered the presumed axisymmetric geometry used in calculating the momentum. In particular, when the local jet axis deviated from the ultrasound plane, the central core of the jet was not imaged, and calculated momentum thus fell. Mathematical simulation of this problem reveals the following reduction in measured momentum (expressed as percent of the true momentum) for a given amount of imaging deviation from the jet axis (expressed as percent of the half velocity radius of the jet): 20% deviation, 5% error; 40% deviation, 20% error; and 60% deviation, 40% error. In practice, it was generally straightforward to identify regions within the jet where significant axial deviation occurred and to exclude these areas from analysis.

In addition to these physical reasons for variance in measured momentum, there are a number of technical limitations in the current generation of color Doppler flow mappers, which have recently been summarized.[2] Among these are the relatively coarse spatial, temporal, and velocity resolution of the instrument. In particular, the finite lateral resolution of contemporary echocardiographic equipment may lead to apparent broadening of the jet with consequent overestimation of momentum when Equa-

tion 2 is applied. Mitigating this effect partially is the fact that this broadened region is at the jet periphery where velocity is the lowest and contributes little to the overall calculation. Velocity aliasing also limits the analysis of high-velocity jets. We attempted only a single unwrapping of the observed data, and so our analysis was limited to regions where velocity was less than twice the Nyquist limit. This limitation may be minimized by using the lowest possible depth setting and carrier frequency and by not analyzing the proximal jet. The future development of a high-pulse repetition Doppler velocity map would help further. Finally, at the aliasing boundaries, there were pixels that contained red and blue information because of either the limited color bandwidth of the NTSC video standard[30] or to signal degradation from the videotape. This red-blue "leakage" led to a velocity discontinuity at the aliasing boundary as shown in Figure 3D. Analysis of direct digital velocities should eliminate this problem.

Extension of momentum analysis to the clinical situation may encounter further difficulties. Cardiac flow is pulsatile, and Equation 3 has been validated only in steady flow. There is a time delay between the onset of flow and full jet development and some persistence of the jet after flow has stopped.[25] These effects appear partially to offset each other, but this must be investigated further. The turbulent nature of these jets will require careful data averaging. Averaging along the jet axis (as was done for the present study) may not be entirely satisfactory in pulsatile flow; gated averaging throughout several cardiac cycles is another approach. The computer memory and processing power necessary for such an algorithm should be routinely available in clinical echocardiographic instruments within a few years.

The present study used round orifices, whereas regurgitant lesions are usually irregular. If the jet is not axisymmetric, then quantification of momentum from a single coaxial plane will not be possible. Fortunately, we have shown that jets originating from elliptical orifices become axisymmetric within 2 cm.[20] More troublesome will be mixing of flows (e.g., mitral regurgitation with pulmonic inflow) and eccentrically directed jets that impinge on adjacent walls (and therefore impart momentum to the wall). Thus, as encouraging as our in vitro results have been, extensive in vivo and clinical validation remain.

### *Other Quantitative Doppler Techniques for Regurgitant Flow*

*Momentum analysis based on centerline velocity.* If jet velocity is given by Equation 3, simplifying momentum calculation may be possible by measuring only the centerline velocity. Along the jet axis, $r=0$ and $e^{-94(r/x)^2}=1$, so $u_m(x)=7.8\sqrt{M}/x$. Squaring this and substituting $M=Q_o u_o$ from Equation 1A yields $u_m^2=60.8Q_o u_o/x^2$, which leads to the simple expression for $Q_o$: $Q_o=u_m^2x^2/60.8u_o$. Thus, by measuring $u_o$ at the orifice with continuous wave Doppler and the axial velocity $u_m$ with pulsed Doppler at a distance x from the orifice, it should be possible to quantify $Q_o$. In vitro validation of an equation of this form was recently reported.[31] However, the considerable instantaneous variance in both the velocity and position of the jet axis noted in the present study emphasizes the need for careful data averaging with this simplified equation.

*Quantifying jet kinetic energy.* Another recent report describes analysis of jet kinetic energy,[32] showing improved characterization of jet severity over simple jet area for situations of changing orifice area, driving pressure, flow rate, size, and compliance of the receiving chamber. Interestingly, the actual calculation performed was to sum the square of the pixel velocities throughout the observed jet, which is similar to the method used in the present study. Velocity squared is the appropriate weighting factor for calculating kinetic energy when the jet is analyzed as a rigid body in classic mechanics (termed "a Lagrangian reference frame"); however, it also is the correct weighting factor when momentum flux is calculated as we have done for the more conventional fluid dynamics analysis with the coordinate system fixed within the moving stream (termed "an Eulerian frame").[33] Two differences, however, should be noted. In the present study, the known axisymmetric geometry of the jet was used to calculate momentum flux within the physical three-dimensional jet, whereas Bolger et al[32] simply summed squared velocity within the observed Doppler flow map without geometric weighting. Theoretical arguments exist in favor of analyzing the jet as a three-dimensional entity as we have done, but the additional computational demands may in part offset this advantage. In addition, we have averaged together the momentum flux at various planes perpendicular to the jet axis, whereas the kinetic energy was summed throughout the jet.

*Proximal flow convergence.* A final recently described approach to Doppler flow quantification involves analysis of the convergence zone proximal to the jet orifice.[34] As blood accelerates toward an obstruction, aliasing has been frequently noted to occur within the proximal chamber, which indicates that at the aliasing point, blood is traveling at the Nyquist velocity, $u_N$. This aliasing surface is in fact a hemisphere surrounding the orifice, with area $2\pi r^2$, where r is the radius of the alias line. By the continuity principle, the flow through this hemisphere, $2\pi u_N r^2$, must be the flow through the orifice. This method is fundamentally different from the above ones, being based on conservation of mass rather than on momentum and is thus a potentially complementary technique. For instance, the convergence zone may be unreliable for small jets where the aliasing radius cannot be resolved; however, we have shown that momentum flux quantification retains accuracy almost to zero flow. Conversely, high-flow and high-velocity jets, whose momentum may be difficult to quantify because of multiple aliasing, may be more easily quantified by using the continuity equation through the convergence zone.

*Summary*

We have shown that the best single parameter to predict the appearance of an axisymmetric jet by color Doppler flow mapping is momentum flux, which combines jet flow rate, velocity, driving pressure, and orifice area into a single number. Unfortunately, although momentum is the optimal jet parameter, the actual observed area of color flow is more influenced by nonjet factors such as chamber constraint and machine gain. Thus, analysis of jet area alone is unlikely to yield quantitative data about jet flow rate.

We have shown, however, that an analysis based on the actual velocities within the jet is more promising. In particular, we showed in vitro that momentum can be accurately measured from the flow map for a wide range of jet severity. Because momentum is also given by the product of orifice velocity and flow rate, we divided the measured momentum within the jet by the orifice velocity and obtained an accurate estimate of the clinically relevant quantity of orifice flow rate. Similarly, momentum was divided by the square of the velocity to yield an estimate for the effective jet orifice area. Although extensive in vivo validation remains, analysis of Doppler flow maps based on conservation of momentum appears to be a theoretically sound and potentially practical method for evaluating the severity of valvular regurgitation.

## Appendix 1

We seek an expression for the area of a color flow jet as a function of jet momentum (M), the low velocity cutoff of the Doppler instrument ($u_c$), and the length of the receiving chamber (the axial cutoff distance, $x_c$). The jet velocity distribution within the receiving chamber will be given by Equation 3:

$$u(x,r)=\frac{7.8\sqrt{M}}{x}e^{-94(r/x)^2}$$

We make the simple assumption that color will be displayed wherever the velocity exceeds $u_c$; that is, inside the contour where $u(x,r)=u_c$.

To describe the jet profile at a given velocity contour, we must invert Equation 3 to express the radius (r) of displayed color as a function of axial distance from the jet origin (x) and $u_c$. After some algebraic manipulation, we obtain

$$r(x,u_c)=x\left(\frac{1}{94}\ln\frac{7.8\sqrt{M}}{u_c x}\right)^{1/2} \quad (A1)$$

$$=\frac{x}{9.7}\left(\ln\frac{7.8\sqrt{M}}{u_c x}\right)^{1/2}$$

Equation A1 looks rather unwieldy, but it is in fact a smooth, well-behaved function.

The displayed length (L) of the color jet (in the absence of chamber constraint) is determined by where the centerline velocity falls below $u_c$ or

$$L=7.8\sqrt{M}/u_c$$

The total area of a free jet is obtained by integrating Equation A1 from 0 to L:

$$JA(M,u_c)=2\int_0^L \frac{x}{9.7}\left(\ln\frac{7.8\sqrt{M}}{u_c x}\right)^{1/2} dx$$

This may be integrated using the substitution $\xi=u_c x/7.8\sqrt{M}$ with the definite integral relation $\int_0^1 \xi[\ln(1/\xi)]^{1/2}\,d\xi=\Gamma(1.5)/2^{1.5}$ to yield*[35]

$$JA=3.93\,M/u_c^2 \quad (A2)$$

Jet area within a constrained chamber of length $x_c$ can be estimated most simply by truncating the jet at $x_c$ cm from the orifice or, in other words, integrating Equation A1 from 0 to $x_c$ rather than 0 to L:

$$JA(M,x_c,u_c)=2\int_0^{x_c} \frac{x}{9.7}\left(\ln\frac{7.8\sqrt{M}}{u_c x}\right)^{1/2} dx$$

This integral is expressible in closed form through a series of substitutions. First, let $\xi=u_c x/7.8\sqrt{M}$ yielding

$$JA=K\int_0^{\xi_c}\xi\sqrt{\ln(1/\xi)}\,d\xi$$

where $K=(2\times7.8^2M)/(9.7u_c^2)=12.5M/u_c^2$ and $\xi_c=u_c x_c/7.8\sqrt{M}$ that ranges from 0 to 1. Next, let $\nu=\sqrt{\ln(1/\xi)}$ yielding

$$JA=2K\int_{\nu_c}^{\infty}\nu^2 e^{-2\nu^2}\,d\nu$$

where $\nu_c=\sqrt{\ln(1/\xi_c)}$, which ranges from 0 for unconstrained jets to $\infty$ for infinitesimally small receiving chambers. This expression may be integrated by parts ($\int u\,dv=uv-\int v\,du$) with $u=\nu$ and $dv=\nu e^{-2\nu^2}\,d\nu$:

$$JA=K[\tfrac{1}{2}\nu_c e^{-2\nu_c^2}+(\sqrt{\pi}/4\sqrt{2})\,\mathrm{erfc}(\sqrt{2}\nu_c)]^*$$

Backsubstituting for $\nu$, $\xi$, and K yields

$$JA(M,x_c,u_c)=\frac{x_c^2}{9.7}\left(\ln\frac{7.8\sqrt{M}}{u_c x_c}\right)^{1/2}$$
$$+\frac{3.93M}{u_c^2}\,\mathrm{erfc}\left[\sqrt{2}\left(\ln\frac{7.8\sqrt{M}}{u_c x_c}\right)^{1/2}\right] \quad (A3)$$

This function is displayed graphically in Figure 7 and discussed in the text.

It should be remembered that this mathematical development assumes that the only effect of chamber constraint is truncation of the jet at the cham-

*$\Gamma(x)$ is the gamma function defined by the integral $\Gamma(x)=\int_0^\infty t^{x-1}e^{-t}dt$, which is related to the factorial function as $n!=\Gamma(n+1)$.

*erfc is the complementary error function, $\mathrm{erfc}(x)=\frac{2}{\sqrt{\pi}}\int_x^\infty e^{-t^2}dt$, familiar from normal (Gaussian) statistics.

ber wall. Modeling the gradual transfer of momentum to the chamber wall would require complex finite element calculations and should not be greatly different from Equation A3.

## References


1. Omoto R, Yokote Y, Takamoto S, Kyo S, Ueda K, Asano H, Namekawa K, Kasai C, Kondo Y, Koyano A: The development of real-time two-dimensional Doppler echocardiography and its clinical significance in acquired valvular diseases: With specific reference to the evaluation of valvular regurgitation. *Jpn Heart J* 1984;25:325–340
2. Sahn DJ: Instrumentation and physical factors related to visualization of stenotic and regurgitant jets by Doppler color flow mapping. *J Am Coll Cardiol* 1988;12:1354–1365
3. Switzer DF, Yoganathan AP, Nanda NC, Woo YR, Ridgway AJ: Calibration of color Doppler flow mapping during extreme hemodynamic conditions in vitro: A foundation for a reliable quantitative grading system for aortic incompetence. *Circulation* 1987;75:837–846
4. Thomas JD, Davidoff R, Wilkins GT, Choong CY, Svizzero T, Weyman AE: The volume of a color flow jet varies directly with flow rate and inversely with orifice size: A hydrodynamic *in vitro* assessment (abstract). *J Am Coll Cardiol* 1988;11:19A
5. Simpson IA, Valdes-Cruz LM, Sahn DJ, Murillo A, Tamura T, Chung KY: Doppler color flow mapping of simulated *in vitro* regurgitant jets: Evaluation of the effects of orifice size and hemodynamic variables. *J Am Coll Cardiol* 1989;13:1195–1207
6. Miyatake K, Izumi S, Okamoto M, Kinoshita N, Asonuma H, Nakagawa H, Yamamoto K, Takamiya M, Sakakibara H, Nimura Y: Semiquantitative grading of severity of mitral regurgitation by real-time two-dimensional Doppler flow imaging technique. *J Am Coll Cardiol* 1986;7:82–88
7. Helmcke F, Nanda NC, Hsiung MC, Soto B, Adey CK, Goyal RG, Gatewood RP: Color Doppler assessment of mitral regurgitation with orthogonal planes. *Circulation* 1987; 75:175–183
8. Perry GJ, Helmcke F, Nanda NC, Byard C, Soto B: Evaluation of aortic insufficiency by Doppler color flow mapping. *J Am Coll Cardiol* 1987;9:952–959
9. Suzuki Y, Kambara H, Kadota K, Tamaki S, Yamazato A, Nohara R, Osakada G, Kawai C: Detection and evaluation of tricuspid regurgitation using a real-time, two-dimensional, color-coded, Doppler flow imaging system: Comparison with contrast two-dimensional echocardiography and right ventriculography. *Am J Cardiol* 1986;57:811–815
10. Howarth L: Concerning the velocity and temperature distributions in plane and axially symmetrical jets. *Proc Cambr Phil Soc* 1938;34:185–203
11. Wygnanski I, Fiedler H: Some measurements in the self-preserving jet. *J Fluid Mechanics* 1969;38:577–612
12. Pai S-I: *Fluid Dynamics of Jets.* New York, McGraw-Hill Book Co, 1979
13. Abramovich GN: *The Theory of Turbulent Jets.* Cambridge, Mass, MIT Press, 1963
14. Schlichting H: *Boundary Layer Theory,* ed 7. New York, McGraw-Hill, 1979
15. Blevins RD: *Applied Fluid Dynamics Handbook.* New York, Van Nostrand Reinhold, 1984, pp 229–247
16. Yoganathan AP, Cape EG, Sung H-W, Williams FP, Jimoh A: Review of hydrodynamic principles for the cardiologist: Applications to the study of blood flow and jets by imaging techniques. *J Am Coll Cardiol* 1988;12:1344–1353
17. Johansen FC: Flow through pipe orifices at low Reynolds number. *Proc R Soc London* 1929;126:231–245
18. Smith RL, Blick EF, Coalson I, Stein PD: Thrombus production by turbulence. *J Appl Physiol* 1972;32:261–264
19. Krabill KA, Sung H-W, Tamura T, Chung KJ, Yoganathan AP, Sahn DJ: Factors influencing the structure and shape of stenotic and regurgitant jets: An *in vitro* investigation using Doppler color flow mapping and optical flow visualization. *J Am Coll Cardiol* 1989;13:1672–1681
20. O'Shea JP, Thomas JD, Popovic AD, Svizzero T, Weyman AE: The profile of a regurgitant color flow jet is independent of orifice shape (abstract). *J Am Coll Cardiol* 1989;13:23A
21. Thomas JD, Weyman AE: A fluid dynamics model of mitral valve flow: Description with *in vitro* validation. *J Am Coll Cardiol* 1989;13:221–233
22. Thomas JD, Wilkins GT, Choong CY, Abascal VM, Palacios IF, Block PC, Weyman AE: Inaccuracy of the mitral pressure half-time immediately following percutaneous mitral valvotomy: Dependence on transmitral gradient and left atrial and ventricular compliance. *Circulation* 1988;78:980–993
23. Thomas JD, Liu C-M, O'Shea JP, Davidoff R, McGlew S, Weyman AE: How turbulent is a turbulent jet? An *in vitro* color flow Doppler study (abstract). *J Am Coll Cardiol* 1989; 13:22A
24. Lobodzinski SM, Ginzton LE, Laks MM: Quantitation of color Doppler images with the color image processor (abstract). *J Am Coll Cardiol* 1988;11:99A
25. Davidoff R, Wilkins GT, Thomas JD, Achorn DM, Weyman AE: Regurgitant volumes by color flow over estimate injected volumes in an *in vitro* model (abstract). *J Am Coll Cardiol* 1987;9:110A
26. Press WH, Flannery BP, Teukolsky SA, Vetterling WT: *Numerical Recipes.* New York, Cambridge University Press, 1986, pp 521–529
27. Mohr-Kahaly S, Lotter R, Brennecke R: Influence of color Doppler instrument setup on the minimal encoded velocity: An *in vitro* study (abstract). *Circulation* 1988;78(suppl II):II-12
28. Stevenson JG: Critical importance of gain, pulse repetition frequency and carrier frequency upon apparent 2D color Doppler jet size (abstract). *Circulation* 1988;78(suppl II):II-12
29. Utsunomiya T, Ogawa T, King SW, Moore GW, Gardin JM: Effect of machine parameters on variance image display in Doppler color flow mapping (abstract). *Circulation* 1988; 78(suppl II):II-12
30. Pratt WK: *Digital Image Processing.* New York, John Wiley & Sons, 1978, pp 593–598
31. Cape EG, Yoganathan AP, Levine RA: A new method for noninvasive quantification of valvular regurgitation based on conservation of momentum: An in vitro validation. *Circulation* 1989;79:1343–1353
32. Bolger AF, Eigler NL, Pfaff JM, Resser KJ, Maurer G: Computer analysis of Doppler color flow mapping images for quantitative assessment of in vitro fluid jets. *J Am Coll Cardiol* 1988;12:450–457
33. Hughes WF, Brighton JA: *Fluid Dynamics.* New York, McGraw-Hill, 1967, p 35
34. Bargiggia G, Recusani F, Yoganathan AP, Valdes-Cruz L, Raisaro A, Simpson IA, Sung HW, Tronconi L, Sahn DJ: Color flow Doppler quantitation of regurgitant flow rate using the flow convergence region proximal to the orifice of a regurgitant jet (abstract). *Circulation* 1988;78(suppl II):II-609
35. Weast RC (ed): *Handbook of Chemistry and Physics.* Cleveland, Ohio, The Chemical Rubber Company, p A-209


KEY WORDS • valvular regurgitation • echocardiography, Doppler • fluid dynamics • computer methods